

## Two mass-scale oscillation analysis of atmospheric and reactor data

M. C. Gonzalez-Garcia<sup>1,2,3,\*</sup> and M. Maltoni<sup>2,†</sup>

<sup>1</sup>*Theory Division, CERN, CH-1211 Geneva 23, Switzerland*

<sup>2</sup>*Instituto de Física Corpuscular, Universitat de València – C.S.I.C.  
Edificio Institutos de Paterna, Apt. 22085, E-46071 Valencia, Spain*

<sup>3</sup>*C.N. Yang Institute for Theoretical Physics  
State University of New York at Stony Brook*

### Abstract

An analysis of atmospheric and reactor neutrino data is presented in terms of three-neutrino oscillations where the effect of both mass differences is explicitly considered. We study the allowed parameter space resulting from this analysis as a function of the *mass splitting hierarchy parameter*  $\alpha = \Delta m^2 / \Delta M^2$  which parametrizes the departure from the one-dominant mass scale approximation. We consider schemes with both direct and inverted mass ordering. Our results show that the analysis of the atmospheric neutrino data does not provide any significant restriction on  $\alpha$  but even for large deviations of the one-dominant mass scale approximation the derived range of the largest mass splitting,  $\Delta M^2$ , is stable while the allowed ranges of mixing angles  $\sin^2 \theta_{23}$  and  $\sin^2 \theta_{13}$  are wider than those obtained in the one-dominant mass scale approximation. Inclusion of the CHOOZ reactor data in the analysis favours small values of  $\alpha$ . This results into the reduction of the parameter space in particular for the mixing angles. As a consequence the final allowed ranges of parameters from the combined analysis are only slightly broader than when obtained in the one-dominant mass scale approximation.

---

\*Electronic address: concha@mail.cern.ch

†Electronic address: maltoni@ific.uv.es

## I. INTRODUCTION

Super-Kamiokande (SK) high statistics data [2] indicate that the observed deficit in the  $\mu$ -like atmospheric events is due to the neutrinos arriving in the detector at large zenith angles, strongly suggestive of the  $\nu_\mu$  oscillation hypothesis. Similarly, their data on the zenith angle dependence and recoil energy spectrum of solar neutrinos [3] in combination with and SNO results [4] and the the results from Homestake [5], SAGE [6], and GALLEX+GNO [7, 8] experiments, have put on a firm observational basis the long-standing problem of solar neutrinos [9], strongly indicating the need for  $\nu_e$  conversions.

Altogether, the solar and atmospheric neutrino anomalies constitute the only solid present-day evidence for physics beyond the Standard Model (SM). It is clear that the minimum joint description of both anomalies requires neutrino conversions among all three known neutrinos. In the simplest case of oscillations the latter are determined by the structure of the lepton mixing matrix [10], which, in addition to the Dirac-type phase analogous to that of the quark sector, contains two physical phases associated to the Majorana character of neutrinos, which however are not relevant for neutrino oscillation and will be set to zero in what follows. In this case the mixing matrix can be conveniently chosen in the form [11]

$$\mathbf{U} = \begin{pmatrix} c_{13}c_{12} & s_{12}c_{13} & s_{13}e^{-i\delta} \\ -s_{12}c_{23} - s_{23}s_{13}c_{12}e^{i\delta} & c_{23}c_{12} - s_{23}s_{13}s_{12}e^{i\delta} & s_{23}c_{13} \\ s_{23}s_{12} - s_{13}c_{23}c_{12}e^{i\delta} & -s_{23}c_{12} - s_{13}s_{12}c_{23}e^{i\delta} & c_{23}c_{13} \end{pmatrix}, \quad (1)$$

where  $c_{ij} \equiv \cos \theta_{ij}$  and  $s_{ij} \equiv \sin \theta_{ij}$ . Thus the parameter set relevant for the joint study of solar and atmospheric conversions becomes six-dimensional: two mass differences, three mixing angles and one CP phase.

Results from the analysis of solar and atmospheric data in the framework of two-neutrino oscillation [12, 13, 14, 15] imply that the required mass differences satisfy

$$\Delta m_\odot^2 \ll \Delta m_{\text{atm}}^2. \quad (2)$$

For sufficiently small  $\Delta m_\odot^2$  the three-neutrino oscillation analysis of the atmospheric neutrino data can be performed in *the one mass scale dominance approximation* neglecting the effect of  $\Delta m_\odot^2$ . In this approximation it follows that the atmospheric data analysis restricts three of the oscillation parameters, namely,  $\Delta m_{31}^2 = \Delta m_{32}^2$ ,  $\theta_{23}$  and  $\theta_{13}$  [15, 16, 17]. Conversely for the solar neutrino analysis the effect of oscillations with  $\Delta m_{\text{atm}}^2$  can be taken to be averaged and solar data constrains  $\Delta m_{21}^2$ ,  $\theta_{12}$  and  $\theta_{13}$  [16, 18]. In this approximation the reactor

neutrino data from CHOOZ provides information on the atmospheric mass difference and the mixing angle  $\theta_{13}$ , and the CP phase  $\delta$  becomes unobservable.

However the assumption of one mass scale dominance may not be a good approximation neither for reactor nor for atmospheric data, in particular for  $\Delta m_{\odot}^2$  in its upper allowed values. Effects of the departure of the one mass scale dominance approximation in the analysis of the CHOOZ reactor data [19] has been included in Ref. [16, 20, 21]. For atmospheric neutrinos in Refs. [15, 23] it was shown that oscillations with two mass scales of the order of  $10^{-3}$  could give a good description of the existing data. The presence of the second mass scale seems to improve the description of the sub-GeV electron distribution [22]. The effects of keeping both mass scales in the description of atmospheric neutrinos has also been discussed in Refs. [24, 25].

To further explore this possibility we present in this work the result of our analysis of the atmospheric and reactor neutrino data in terms of three-neutrino oscillations where the effect of both mass differences is explicitly considered. We study the allowed parameter space as a function of the ratio between the two mass scales. For atmospheric neutrinos we include in our analysis all the contained events from the latest 79.5 kton-yr SK data set [2], as well as the upward-going neutrino-induced muon fluxes from both SK and the MACRO detector [26].

The outline of this paper is as follows. In Sec. II we describe our notation for the parameters relevant for atmospheric and reactor neutrino oscillations with two mass scales and discuss the results for the relevant probabilities. In Sec. III and IV we show our results for the analysis of atmospheric neutrino and reactor data respectively. The results for the combined analysis are described in Sec. V. Finally in Sec. VI we summarize the work and present our conclusions.

## II. THREE NEUTRINO OSCILLATIONS WITH TWO MASS SCALES

In this section we review the theoretical calculation of the conversion probabilities for atmospheric and reactor neutrinos in the framework of three-neutrino mixing, in order to set our notation and to clarify the approximations used in the evaluation of such probabilities.

In general, the determination of the oscillation probabilities for atmospheric neutrinos require the solution of the Schrödinger evolution equation of the neutrino system in the Earth-matter background. For a three-flavour scenario, this equation reads

$$i \frac{d\vec{\nu}}{dt} = \mathbf{H} \vec{\nu}, \quad \mathbf{H} = \mathbf{U} \cdot \mathbf{H}_0^d \cdot \mathbf{U}^\dagger + \mathbf{V}, \quad (3)$$

where  $\mathbf{U}$  is the unitary matrix connecting the flavour basis and the mass basis in vacuum and which can be parametrized as in Eq. (1). On the other hand  $\mathbf{H}_0^d$  and  $\mathbf{V}$  are given as

$$\mathbf{H}_0^d = \frac{1}{2E_\nu} \mathbf{diag} (0, \Delta m_{21}^2, \Delta m_{31}^2), \quad (4)$$

$$\mathbf{V} = \mathbf{diag} (\pm \sqrt{2} G_F N_e, 0, 0), \quad (5)$$

where  $\vec{\nu} \equiv (\nu_e, \nu_\mu, \nu_\tau)$ . We have denoted by  $\mathbf{H}_0^d$  the vacuum Hamiltonian, while  $\mathbf{V}$  describes charged-current forward interactions in matter. In Eq. (5), the sign  $+$  ( $-$ ) refers to neutrinos (antineutrinos),  $G_F$  is the Fermi coupling constant and  $N_e$  is electron number density in the Earth.

The angles  $\theta_{ij}$  can be taken without any loss of generality to lie in the first quadrant  $\theta_{ij} \in [0, \pi/2]$ . Concerning the CP violating phase  $\delta$  there are two possibilities (for a recent discussion see, for instance [27])

- $0 \leq \delta < 2\pi$ . In this case the full parameter space is covered while keeping the order of masses as  $m_1 \leq m_2 \leq m_3$
- $0 \leq \delta \leq \pi$  and two choices of mass ordering (See Fig. 1) one with  $m_1 \leq m_2 \leq m_3$  which we will denote as *Normal* and other with  $m_3 \leq m_1 \leq m_2$  which we will denote as *Inverted*.

For convenience we will use this second notation. We define as  $\Delta M^2 > 0$  the *large* mass splitting in the problem and  $\Delta m^2 > 0$  the *small* one. In this case we can have the two mass ordering:

$$\text{Normal: } \Delta M^2 = \Delta m_{31}^2 = m_3^2 - m_1^2 \quad \Delta m^2 = \Delta m_{21}^2 = m_2^2 - m_1^2, \quad (6)$$

$$\text{Inverted: } \Delta M^2 = -\Delta m_{32}^2 = m_2^2 - m_3^2 \quad \Delta m^2 = \Delta m_{21}^2 = m_2^2 - m_1^2. \quad (7)$$

Alternatively one could chose, for instance, for the inverted case the mass ordering  $m_3 \leq m_2 \leq m_1$  and in this case

$$\text{Inverted': } \Delta M^2 = -\Delta m_{31}^2 = m_1^2 - m_3^2 \quad \Delta m^2 = -\Delta m_{21}^2 = m_1^2 - m_2^2 \quad (8)$$

which is equivalent to the Inverted scheme in Eq. (8) with  $\theta'_{12} = \frac{\pi}{2} + \theta_{12}$ .

We define the *mass splitting hierarchy parameter*

$$\alpha = \frac{\Delta m^2}{\Delta M^2}, \quad (9)$$

which parametrizes the departure from the one-dominant mass scale approximation in the analysis of atmospheric and reactor neutrinos.

In this convention, for both Normal or Inverted schemes, the mixing angles in Eq. (1) are such that in the one mass dominance approximation in which  $\Delta M^2$  ( $\Delta m^2$ ) determines the oscillation length of atmospheric (solar) neutrinos,  $\theta_{23}$  is the mixing angle relevant for atmospheric oscillations while  $\theta_{12}$  is the relevant one for solar oscillations, and  $\theta_{13}$  is mostly constrained by reactor data. In the likely situation in which the solar solution is LMA,  $\theta_{12}$  is mainly restricted to lie in the first octant.

We will restrict ourselves to the CP conserving scenario. CP conservation implies that the lepton phase  $\delta$  is either zero or  $\pi$  [28]. As we will see, for non-vanishing  $\alpha$  and  $\theta_{13}$  the analysis of atmospheric neutrinos is not exactly the same for these two possible CP conserving values of  $\delta$  and we characterize these two possibilities in terms of  $\cos \delta = \pm 1$ . Alternatively  $\delta$  could be chosen to be restricted to lie in the first quadrant  $0 \leq \delta \leq \frac{\pi}{2}$  at the price of allowing one of the three mixing angles to vary in the range  $[-\frac{\pi}{2}, \frac{\pi}{2}]$ .

For  $\alpha = \theta_{13} = 0$ , atmospheric neutrinos involve only  $\nu_\mu \rightarrow \nu_\tau$  conversions, and in this case there are no matter effects, so that the solution of Eq. (3) is straightforward and the conversion probability takes the well-known vacuum form

$$P_{\mu\mu} = 1 - \sin^2(2\theta_{23}) \sin^2\left(\frac{\Delta M^2 L}{4E_\nu}\right), \quad (10)$$

where  $L$  is the path-length travelled by neutrinos of energy  $E_\nu$ .

On the other hand, in the general case of three-neutrino scenario with  $\theta_{13} \neq 0$  or  $\alpha \neq 0$  the presence of the matter potentials become relevant and it requires a numerical solution of the evolution equations in order to obtain the oscillation probabilities for atmospheric neutrinos  $P_{\alpha\beta}$ , which are different for neutrinos and anti-neutrinos because of the reversal of sign in Eq. (5). In our calculations, we use for the matter density profile of the Earth the approximate analytic parametrization given in Ref. [29] of the PREM model of the Earth [30].

In Figs. 2 and 3 we plot the angular distribution of atmospheric  $\nu_e$  and  $\nu_\mu$  for non-vanishing values of  $\alpha$  or  $\theta_{13}$  obtained from our numerical calculations. As seen in these figures the main effect of a small but non-vanishing  $\alpha$  is mostly observable for sub-GeV electrons, although some effect is also visible for multi-GeV electrons and sub-GeV muons, and it can result either in an increase or in a decrease of the expected number of events with respect to the  $\alpha = 0$  prediction depending on whether  $\theta_{23}$  is in the first or second octant. This behaviour can be understood in terms of the approximate analytical expressions derived

in Ref. [22] (for  $\theta_{13} = 0$ )

$$\frac{N_e}{N_{e0}} - 1 = \bar{P}_{e2}\bar{r}(c_{23}^2 - \frac{1}{\bar{r}}) \quad (11)$$

$$\frac{N_\mu - N_\mu(\alpha = 0)}{N_{\mu0}} = -\bar{P}_{e2}c_{23}^2(c_{23}^2 - \frac{1}{\bar{r}}) \quad (12)$$

where  $N_{e0}$  and  $N_{\mu0}$  are the expected number of electron and muon-like events in the absence of oscillations in the relevant energy and angular bin and  $\bar{r} = N_{\mu0}/N_{e0}$ . For instance, for sub-GeV events  $\bar{r} \sim 2$ . Here  $N_\mu(\alpha = 0)$  is the expected number of muon-like events for  $\alpha = 0$  and  $\bar{P}_{e2}$  is the dominant  $\alpha$ -dependent term in the probabilities, averaged over energy and zenith angle. For neutrinos we have:

$$\begin{aligned} P_{e2} &= \sin^2 2\theta_{12,m} \sin^2 \left( \frac{\Delta m^2 L}{4E_\nu} \frac{\sin 2\theta_{12}}{\sin 2\theta_{12,m}} \right), \\ \sin 2\theta_{12,m} &= \frac{\sin 2\theta_{12}}{\sqrt{(\cos 2\theta_{12} - 2E_\nu V_e / \Delta m^2)^2 + (\sin 2\theta_{12})^2}}, \end{aligned} \quad (13)$$

which for  $\Delta m^2 \ll 2E_\nu V_e$  reduces to:

$$P_{e2} = \alpha^2 \sin^2 2\theta_{12} \left( \frac{\Delta M^2}{2EV_e} \right)^2 \sin^2 \frac{V_e L}{2}. \quad (14)$$

According to Eqs. (11) and (12) the sign of the shift in the number of predicted events with respect to the results in the one mass scale dominance approximation is opposite for electron and muon-like events and it depends on the factor  $c_{23}^2 - \frac{1}{\bar{r}} \sim c_{23}^2 - 0.5$ . So for  $\theta_{23}$  in the first octant,  $c_{23}^2 > 0.5$ , there is an increase (decrease) in the number of electron (muon) events as compared to the  $\alpha = 0$  case. For  $\theta_{23}$  in the second octant the opposite holds. We also see that the net shift is larger for electron events than for muon events by a factor  $c_{23}^2/\bar{r}$ . At higher energies, for up-going muons the effect is negligible.

For the sake of comparison we also show in the figures the behaviour with non-vanishing value of  $\theta_{13}$  in the one mass scale dominance approximation. As seen in the figure the effect is most important for the electron events and can be understood as follows. For the case of constant matter density the expected flux of  $\nu_e$  events in the one mass scale dominance approximation is given by

$$\frac{N_e}{N_{e0}} - 1 = \bar{P}_{e\mu}\bar{r}(s_{23}^2 - \frac{1}{\bar{r}}) \quad (15)$$

where

$$P_{e\mu} = 4s_{13,m}^2 c_{13,m}^2 \sin^2 \left( \frac{\Delta M^2 L}{4E_\nu} \frac{\sin 2\theta_{13}}{\sin 2\theta_{13,m}} \right), \quad (16)$$

$$\sin 2\theta_{13,m} = \frac{\sin 2\theta_{13}}{\sqrt{(\cos 2\theta_{13} \mp 2E_\nu V_e / \Delta M^2)^2 + (\sin 2\theta_{13})^2}} \quad (17)$$

and the  $-$   $(+)$  sign applies for the Normal (Inverted) case. So for  $\theta_{23}$  in the first octant ( $s_{23}^2 < 0.5$ ) there is a decrease in the number of electron events as compared to the  $\theta_{13}$  case. For sub-GeV events, the matter term in Eq. (17) can be neglected and the effect of a non-vanishing  $\theta_{13}$  is the same for Normal and Inverted ordering. For multi-GeV and upgoing muon events matter effects start playing a role and the effect becomes slightly larger for the Normal case where the matter enhancement is in the neutrino channel.

The situation becomes more involved when both  $\alpha$  and  $\theta_{13}$  are different from zero. For instance, in lowest order in  $\alpha$   $s_{13}$  the expected number of sub-GeV  $\nu_e$  events is (after averaging the  $\Delta M^2 L/E$  oscillations)

$$\begin{aligned} \frac{N_e}{N_{e0}} - 1 &= \overline{P}_{e2} \bar{r} (c_{23}^2 - \frac{1}{\bar{r}}) + \overline{P}_{e\mu} \bar{r} (s_{23}^2 - \frac{1}{\bar{r}}) \\ &+ \frac{\bar{r}}{2} \cos \delta \sin 2\theta_{13} \sin 2\theta_{23} \sin 2\bar{\theta}_{12,m} \cos 2\bar{\theta}_{12,m} \overline{\sin^2 \left( \frac{\Delta m^2 L}{4E_\nu} \frac{\sin 2\theta_{12}}{\sin 2\theta_{12,m}} \right)} \end{aligned} \quad (18)$$

and from this equation we see that the *interference* term (the third term in the right hand side) can have either sign depending on  $\cos \delta$ . It also changes sign depending on whether the  $\Delta m^2$  oscillations are above ( $\Delta m^2 \cos 2\theta_{12} > 2E_\nu V_e$ ) or below ( $\Delta m^2 \cos 2\theta_{12} < 2E_\nu V_e$ ) the resonance. For very small  $\alpha$  ( $\Delta m^2 \ll 2E_\nu V_e$ ) the interference term is proportional to  $\alpha$  and it also changes sign for neutrinos and antineutrinos. In summary the effect of non-vanishing  $\theta_{13}$  and  $\alpha$  in the expected number and distribution of atmospheric neutrino events can have opposite signs and this can lead to a partial cancellation between both contributions. This results into a loss of sensitivity of the analysis to both parameters.

To analyze the CHOOZ constraints we need to evaluate the survival probability for  $\bar{\nu}_e$  of average energy  $E \sim$  few MeV at a distance of  $L \sim 1$  Km. For these values of energy and distance, one can safely neglect Earth matter effects. The survival probability takes the analytical form:

$$\begin{aligned} P_{ee}^{\text{CHOOZ}} &= 1 - \cos^4 \theta_{13} \sin^2 2\theta_{12} \sin^2 \left( \frac{\Delta m_{21}^2 L}{4E_\nu} \right) \\ &- \sin^2 2\theta_{13} \left[ \cos^2 \theta_{12} \sin^2 \left( \frac{\Delta m_{31}^2 L}{4E_\nu} \right) + \sin^2 \theta_{12} \sin^2 \left( \frac{\Delta m_{32}^2 L}{4E_\nu} \right) \right] \\ &\simeq 1 - \sin^2 2\theta_{13} \sin^2 \left( \frac{\Delta M^2 L}{4E_\nu} \right), \end{aligned} \quad (19)$$

where the second equality holds under the approximation  $\Delta m^2 \ll E_\nu/L$  which can only be safely made for  $\Delta m^2 \lesssim 3 \times 10^{-4}$  eV $^2$ . Eq. (19) is valid for both Normal and Inverted ordering with the identifications in Eq.(6) and Eq.(7) respectively. It results that the probability for Normal and Inverted schemes is the same with the exchange  $\sin^2 \theta_{12} \leftrightarrow \cos^2 \theta_{12}$ . Thus in

general the analysis of the CHOOZ reactor data involves four oscillation parameters:  $\Delta M^2$ ,  $\theta_{13}$ ,  $\Delta m^2$ , and  $\theta_{12}$ . From Eq. (19) we see that for a given value of  $\theta_{12}$  and  $\Delta M^2$  the effect of a non-vanishing value of either  $\theta_{13}$  or  $\Delta m^2$  is the decrease of the survival probability.

### III. ATMOSPHERIC NEUTRINO ANALYSIS

In our statistical analysis of the atmospheric neutrino events we use all the samples of SK data:  $e$ -like and  $\mu$ -like samples of sub- and multi-GeV [2] data, each given as a 5-bin zenith-angle distribution<sup>1</sup>, and upgoing muon data including the stopping (5 bins in zenith angle) and through-going (10 angular bins) muon fluxes. We have also included the latest MACRO [26] upgoing muon samples, with 10 angular bins. So we have a total of 45 independent inputs.

For details on the statistical analysis applied to the different observables, we refer to the first reference in Ref. [14] and [16]. As discussed in the previous section, the analysis of the atmospheric neutrino data for three neutrino oscillations with two mass scales involves six parameters: two mass differences, three mixing angles and one CP phase. In what follows, for the sake of simplicity, we will restrict ourselves to the CP conserving scenario but we will distinguish the two possible CP conserving values of  $\delta$  and we characterize these two possibilities in terms of  $\cos \delta = \pm 1$ . We will show the results for Normal and Inverted schemes. Furthermore in most of our study we will keep the mixing angle  $\theta_{12}$  fix to its best fit value from the global analysis of solar neutrino data  $\tan^2 \theta_{12} = 1/3$  [12]. With this restrictions our parameter space is four-dimensional. Our aim is to study the modification on the resulting allowed ranges of the parameters  $\Delta M^2$ ,  $\sin^2 \theta_{23}$  and  $\sin^2 \theta_{13}$  due to the deviations from the one-dominant mass scale approximation, *i.e.* for  $\Delta m^2 \neq 0$  (or equivalently for non-vanishing values of mass splitting hierarchy parameter  $\alpha$ ).

We first present the results of the allowed parameters for the global combination of atmospheric observables. Notice that since the parameter space we study is four-dimensional the allowed regions for a given CL are defined as the set of points satisfying the condition for four degrees of freedom (d.o.f.)

$$\chi_{\text{atm}}^2(\Delta M^2, \theta_{23}, \theta_{13}, \Delta m^2) - \chi_{\text{atm,min}}^2 \leq \Delta \chi^2(\text{CL}, 4 \text{ d.o.f.}) \quad (20)$$

where  $\Delta \chi^2(\text{CL}, 4 \text{ d.o.f.}) = 7.78, 9.49, 13.3$  and  $16.25$  for  $\text{CL} = 90\%, 95\%, 99\%$  and  $99.73\% \equiv$

---

<sup>1</sup> Note that for convenience and maximal statistical significance we prefer to bin the SK contained event data in 5, instead of 10 bins.

$3\sigma$  respectively, and  $\chi_{\text{atm,min}}^2$  is the global minimum in the four-dimensional space. The best fit point used to define the allowed parameter space is found to be:

$$\begin{aligned}
\Delta M^2 &= 3.02 \times 10^{-3} \text{ eV}^2 \\
\sin^2 \theta_{23} &= 0.35 \\
\sin^2 \theta_{13} &= 0.1 \\
\Delta m^2 &= 4.5 \times 10^{-4} \text{ eV}^2 \quad (\alpha = 0.15) \\
\chi_{\text{atm,min}}^2 &= 25.8
\end{aligned} \tag{21}$$

and it corresponds to  $\cos \delta = 1$  and the Inverted ordering. For Inverted ordering and  $\cos \delta = 1$  the  $\sin \theta_{13}$  and the  $\sin^2 \theta_{13}$  terms in Eq. (18) can almost cancel each other for  $\theta_{23}$  in the first octant, and this allows for a good description of the sub-GeV electrons with both relatively large  $\alpha$  and  $\theta_{13}$ . This cancellation could also be possible for the Normal ordering but in this case such large values of  $\theta_{13}$  worsen the description of the Multi-GeV and upgoing- $\mu$  events because for the Normal ordering the effect of  $\theta_{13}$  in the distribution of higher energy events is enhanced by matter effects. We find that for the Normal ordering, small values of  $\theta_{13}$  are favoured. As a consequence the best fit point within the Normal ordering is slightly worse with  $\chi_{\text{NOR,min}}^2 = 26.5$  (at  $\Delta M^2 = 2.75 \times 10^{-3} \text{ eV}^2$ ,  $\sin^2 \theta_{23} = 0.375$ ,  $\sin^2 \theta_{13} = 0.005$  and  $\alpha = 0.15$ ), although the difference is not statistically significant.

This result can be compared with the best fit point obtained in the one-dominant mass scale approximation  $\alpha = 0$

$$\begin{aligned}
\Delta M^2 &= 2.5 \times 10^{-3} \text{ eV}^2 \\
\sin^2 \theta_{23} &= 0.44 (\sim 0.56) \\
\sin^2 \theta_{13} &= 0.005 \\
\chi_{\text{atm,min}}^2 &= 28.3
\end{aligned} \tag{22}$$

which is independent of the choice  $\cos \delta = \pm 1$  and given the small value of  $\sin^2 \theta_{13}$  is almost the same for Normal or Inverted schemes and independent of the octant of  $\theta_{23}$ .

In summary, we find that allowing for a non-zero value of  $\alpha$  moderately improves the quality of the global fit. This result is driven by the better description of the sub-GeV data which is attainable for a non-zero  $\alpha$  value, and drives the best fit point to the first octant of the mixing angle  $\theta_{23}$  for which the expected number of sub-GeV electrons is larger as compared to the pure  $\nu_\mu \rightarrow \nu_\tau$  scenario, as illustrated in Figs. 2 and 3. Furthermore for the Inverted case an improved fit to multi-GeV electrons and muons is obtained for a non-vanishing value of  $\theta_{13}$ . We find, however, that the analysis of the atmospheric neutrino data

does not show a strong dependence on large  $\alpha$  values. In Fig. 4 we show the dependence of  $\Delta\chi^2_{\text{atm}}$  on  $\alpha$ . In this plot all the neutrino oscillation parameters which are not displayed have been “integrated out”, *i.e.* the  $\Delta\chi^2$  function is minimized with respect to all the non-displayed variables. From this figure we see that the fit to atmospheric neutrinos is only mildly sensitive to the value of  $\alpha$ .

In Figs. 5–7 we present sections of the allowed volume in the plane  $(\cos\delta\sin^2\theta_{23}, \Delta M^2)$  for different values of  $\sin^2\theta_{13}$ . In the different figures we display the corresponding sections for the Normal and Inverted schemes and for values of  $\Delta m^2 = 0$ ,  $\Delta m^2 = 5.2 \times 10^{-5} \text{ eV}^2$  (best fit point from the present analysis of the solar neutrino data including the data of 1496 days of SK [31]),  $\Delta m^2 = 8 \times 10^{-4} \text{ eV}^2$  (maximum allowed value by present analysis of the reactor and solar neutrino data). For illustration we also show in Fig. 8 the corresponding regions for the “democratic” scenario  $\alpha = 0.5$  ( $\Delta m^2 = \Delta M^2/2$ ).

Comparing Fig. 5 for  $\alpha = 0$  with the corresponding figures for non vanishing  $\alpha$  values we find that already for  $\Delta m^2 = 5.2 \times 10^{-5}$  there appear differences although only for large values of  $\theta_{13}$ . However from these figures one also realizes that even for large values of  $\alpha$  the allowed region does not extend to a very different range of  $\Delta M^2$ . Conversely, the mixing angles  $\theta_{23}$  and  $\theta_{13}$  can become less constrained when the case  $\alpha \neq 0$  is considered.

To further quantify these effects we plot in Figs. 9–11 the dependence of  $\Delta\chi^2_{\text{atm}}$  on  $\Delta M^2$ ,  $\theta_{23}$  and  $\theta_{13}$ , respectively, for different values of  $\alpha$ , after minimizing with respect to all the non-displayed variables. From these figures we can read the  $3\sigma$  allowed ranges for the different parameters (1 d.o.f.):

For arbitrary $\alpha$		
Normal	Inverted	
$1.3 \leq \frac{\Delta M^2}{10^{-3} \text{ eV}^2} \leq 8.8$	$1.2 \leq \frac{\Delta M^2}{10^{-3} \text{ eV}^2} \leq 13.6$	
$0.18 \leq \sin^2\theta_{23} \leq 0.79$	$0.07 \leq \sin^2\theta_{23} \leq 0.80$	for $\cos\delta = 1$
$0.17 \leq \sin^2\theta_{23} \leq 0.79$	$0.18 \leq \sin^2\theta_{23} \leq 0.98$	for $\cos\delta = -1$
$\sin^2\theta_{13} \leq 0.46$	$\sin^2\theta_{13} \leq 1$	for $\cos\delta = 1$
$\sin^2\theta_{13} \leq 0.26$	$\sin^2\theta_{13} \leq 1$	for $\cos\delta = -1$

For  $\alpha = 0$

Normal	Inverted	
$1.1 \leq \frac{\Delta M^2}{10^{-3} \text{ eV}^2} \leq 6.7$	$1.1 \leq \frac{\Delta M^2}{10^{-3} \text{ eV}^2} \leq 7.5$	(24)
$0.26 \leq \sin^2 \theta_{23} \leq 0.82$	$0.26 \leq \sin^2 \theta_{23} \leq 0.83$	for $\cos \delta = \pm 1$
$\sin^2 \theta_{13} \leq 0.34$	$\sin^2 \theta_{13} \leq 0.52$	for $\cos \delta = \pm 1$

Comparing the ranges in Eqs. (23) and (24) we see that the parameter which is less sensitive to the departure from the one mass scale dominance approximation is  $\Delta M^2$ , while  $\sin^2 \theta_{13}$  is the mostly affected, in particular for the inverted scheme for which no upper bound on  $\sin^2 \theta_{13}$  is derived from the analysis. The careful reader may notice that for the Normal ordering, the bound on  $\theta_{13}$  for arbitrary  $\alpha$  can be stronger than for  $\alpha = 0$ . This is due to the fact that the ranges in Eqs. (23) and (24) are defined in terms of  $3\sigma$  shifts in the  $\chi^2$  function with respect to the minima in Eqs. (21) and (22) respectively.

Finally we show in Fig. 12 the 2-dimensional allowed regions in  $(\cos \delta \sin^2 \theta_{23}, \Delta M^2)$  from the analysis of the atmospheric neutrino data independently of the values of  $\alpha$  and  $\theta_{13}$ . In constructing these regions for each value of  $\Delta M^2$  and  $\cos \delta \sin^2 \theta_{23}$  we have minimized on the oscillation parameters  $\Delta m^2$  and  $\theta_{13}$  so the they are defined in terms of  $\Delta \chi^2$  for 2 d.o.f. ( $\Delta \chi^2 = 4.61, 5.99, 9.21, 11.8$  for 90%, 95%, 99% CL and  $3\sigma$  respectively). For the sake of comparison we show in the figure the corresponding regions for  $\alpha = 0$ . From the figure we see that the differences are larger for the Inverted scheme.

#### IV. ANALYSIS OF CHOOZ DATA

The CHOOZ experiment [19] searched for disappearance of  $\bar{\nu}_e$  produced in a power station with two pressurized-water nuclear reactors with a total thermal power of 8.5 GW (thermal). At the detector, located at  $L \simeq 1$  Km from the reactors, the  $\bar{\nu}_e$  reaction signature is the delayed coincidence between the prompt  $e^+$  signal and the signal due to the neutron capture in the Gd-loaded scintillator. Their measured vs. expected ratio, averaged over the neutrino energy spectrum is

$$R = 1.01 \pm 2.8\%(\text{stat}) \pm 2.7\%(\text{syst}) . \quad (25)$$

Thus no evidence was found for a deficit of measured vs. expected neutrino interactions, and they derive from the data exclusion plots in the plane of the oscillation parameters ( $\Delta m^2, \sin^2 2\theta$ ) in the simple two-neutrino oscillation scheme. At 90% CL they exclude the region given approximately by  $\Delta m^2 > 7 \cdot 10^{-4} \text{ eV}^2$  for maximum mixing, and by  $\sin^2(2\theta) >$

0.10 for large  $\Delta m^2$ .

In order to combine the CHOOZ bound with the results from our analysis of atmospheric neutrino data in the framework of three-neutrino mixing we have first performed our own analysis of the CHOOZ data. Using as experimental input their measured ratio (25) [19] and comparing it with the theoretical expectations we define the  $\chi^2_{\text{CHOOZ}}$  function. As discussed in Sec. II for the analysis of the reactor data the relevant oscillation probability depends in general on the four parameters  $\theta_{12}$ ,  $\Delta m^2$ ,  $\theta_{13}$ , and  $\Delta M^2$ . In Fig. 13 we show the excluded regions at 90, 95 and 99% CL and  $3\sigma$  in the  $(\sin^2 \theta_{13}, \Delta M^2)$  plane from our analysis of the CHOOZ data for several values of  $\Delta m^2$  and  $\tan^2 \theta_{12} = 1/3$ ; for the sake of comparison with the 2-family analysis we have defined the allowed regions for 2 d.o.f. ( $\Delta \chi^2_{\text{CHOOZ}} = 4.61, 5.99, 9.21, 11.83$  respectively). In the left (right) panel we show the results for the Normal (Inverted) scheme. We see that the presence of a non-vanishing value of  $\Delta m^2$  results into a slightly smaller allowed range of  $(\Delta M^2, \sin^2 \theta_{13})$ . For the chosen value of  $\tan^2 \theta_{12}$  the reduction for smaller values of  $\Delta M^2$  is slightly more significant for the Normal than for the Inverted scheme as also shown in Ref. [20]. This can be easily understood from the expression of the survival probability: from Eq. (19), we get

$$P_{ee,\text{NOR}}^{\text{CHOOZ}} - P_{ee,\text{INV}}^{\text{CHOOZ}} = -\sin^2 2\theta_{13}(\cos^2 \theta_{12} - \sin^2 \theta_{12}) \left[ \sin^2 \left( \frac{\Delta M^2 L}{4E_\nu} \right) - \sin^2 \left( \frac{(\Delta M^2 - \Delta m^2)L}{4E_\nu} \right) \right] < 0 \text{ for } \theta_{12} \leq \frac{\pi}{4}, \quad (26)$$

so for  $\theta_{12} \leq \frac{\pi}{4}$  the survival probability is smaller for the Normal ordering than for the Inverted one, which leads to the stronger constraint. For  $\Delta M^2 \gg \Delta m^2$ , Eq. (26) vanishes and the excluded regions in the two schemes become indistinguishable.

## V. COMBINED ANALYSIS

We now describe the effect of including the CHOOZ reactor data together with the atmospheric data samples in a combined 3-neutrino  $\chi^2$  analysis. The results of this analysis are summarized in Fig. 4 and in Figs. 14–17. As in Sec. III in most of results shown here we fix the mixing angle  $\tan^2 \theta_{12} = 1/3$  and study the allowed ranges of the parameters  $\Delta M^2$ ,  $\sin^2 \theta_{23}$  and  $\sin^2 \theta_{13}$  on  $\alpha$ .

We find that, in this case, the best fit point for the combined analysis of atmospheric and CHOOZ data corresponds to Inverted schemes with:

$$\Delta M^2 = 2.5 \times 10^{-3} \text{ eV}^2$$

$$\begin{aligned}
\sin^2 \theta_{23} &= 0.375 \\
\sin^2 \theta_{13} &= 0.0 \\
\Delta m^2 &= 2.5 \times 10^{-4} \text{ eV}^2 \quad (\alpha = 0.1) \\
\chi^2_{\text{atm+CHOOZ,min}} &= 27.0
\end{aligned} \tag{27}$$

and  $\cos \delta = \pm 1$ . Normal schemes lead to a equally good fit but for  $\Delta M^2 = 2.75 \times 10^{-3} \text{ eV}^2$ .

For  $\alpha = 0$  the best fit point is at:

$$\begin{aligned}
\Delta M^2 &= 2.5 \times 10^{-3} \text{ eV}^2 \\
\sin^2 \theta_{23} &= 0.44 (\sim 0.56) \\
\sin^2 \theta_{13} &= 0.005 \\
\chi^2_{\text{atm+CHOOZ,min}} &= 28.5
\end{aligned} \tag{28}$$

In Fig. 4 we show the dependence of  $\Delta \chi^2_{\text{atm+CHOOZ}}$  on  $\alpha$ . From this figure we see that the inclusion of the CHOOZ reactor data results into a stronger dependence of the analysis on the value of  $\Delta m^2$  (or equivalently on  $\alpha$ ) and large values of the mass splitting hierarchy parameter become disfavoured. Also the dependence is stronger for the Normal scheme, as expected (see discussion below Eq. (26)). As a consequence the ranges of mixing parameters – which, in the analysis of atmospheric data alone, were broaden in presence of large values of  $\alpha$  – are expected to become narrower with the inclusion of the CHOOZ data in the analysis.

This effect is explicitly shown in Figs. 14–16, where we plot the dependence of the  $\Delta \chi^2_{\text{atm+CHOOZ}}$  on  $\Delta M^2$ ,  $\theta_{23}$  and  $\theta_{13}$ , respectively, for different values of  $\alpha$  (to be compared with the corresponding Figs. 9–11 for the analysis of the atmospheric data). The figures illustrate that indeed the inclusion of the CHOOZ data in the analysis results into a reduction of the allowed ranges for the mixing angles, in particular  $\theta_{13}$ .

From these figures we also read the  $3\sigma$  allowed (1 d.o.f.) bounds:

For arbitrary $\alpha$		
Normal	Inverted	
$1.2 \leq \frac{\Delta M^2}{10^{-3} \text{ eV}^2} \leq 5.7$	$1.1 \leq \frac{\Delta M^2}{10^{-3} \text{ eV}^2} \leq 5.5$	
$0.19 \leq \sin^2 \theta_{23} \leq 0.75$	$0.19 \leq \sin^2 \theta_{23} \leq 0.74$	for $\cos \delta = 1$
$0.19 \leq \sin^2 \theta_{23} \leq 0.75$	$0.19 \leq \sin^2 \theta_{23} \leq 0.74$	for $\cos \delta = -1$
$\sin^2 \theta_{13} \leq 0.06$	$\sin^2 \theta_{13} \leq 0.09$	for $\cos \delta = 1$
$\sin^2 \theta_{13} \leq 0.06$	$\sin^2 \theta_{13} \leq 0.08$	for $\cos \delta = -1$

For  $\alpha = 0$

Normal	Inverted	
$1.1 \leq \frac{\Delta M^2}{10^{-3} \text{ eV}^2} \leq 5.4$	$1.1 \leq \frac{\Delta M^2}{10^{-3} \text{ eV}^2} \leq 5.3$	(30)
$0.25 \leq \sin^2 \theta_{23} \leq 0.77$	$0.26 \leq \sin^2 \theta_{23} \leq 0.76$	for $\cos \delta = \pm 1$
$\sin^2 \theta_{13} \leq 0.07$	$\sin^2 \theta_{13} \leq 0.07$	for $\cos \delta = \pm 1$

Comparing with the results in Eq. (23) we see that including the CHOOZ reactor data reduces the effect on the final allowed range of parameters arising from allowing departures from the one mass scale dominance approximation. In other words the ranges in Eq. (29) and (30) are not very different.

Fig. 17 shows the global 2-dimensional allowed regions in  $(\cos \delta \sin^2 \theta_{23}, \Delta M^2)$  from the analysis of the atmospheric neutrino and CHOOZ reactor data for optimized values  $\alpha$  and  $\theta_{13}$  as well as the results for the one mass scale dominance approximation  $\alpha = 0$  case. Comparison with Fig. 12 shows that the after including the CHOOZ reactor data the allowed range of parameters  $\Delta M^2$  and  $\sin^2 \theta_{23}$  becomes more “robust” and it is almost independent of the Normal or Inverted ordering of the masses or of the particular choice of  $\cos \delta = \pm 1$ .

## VI. SUMMARY

In this article we have explored the effect of keeping the two mass scales on the three-flavour oscillation analysis of the atmospheric and reactor neutrino data. In general the analysis of atmospheric data involves six parameters: two mass differences, which we denote by  $\Delta M^2$  and  $\Delta m^2$ , three mixing angles ( $\theta_{23}$ ,  $\theta_{13}$  and  $\theta_{12}$ ) and one CP phase ( $\delta$ ). The analysis of the reactor data involves four of these parameters, namely,  $\Delta M^2$  and  $\delta m^2$ ,  $\theta_{13}$  and  $\theta_{12}$ . For the sake of simplicity we have concentrated on the CP conserving scenario, thus allowing only two possible values of the CP conserving phase, and we have studied the results for both Normal and Inverted mass schemes.

First we have performed the independent analyses of the atmospheric neutrino data and of the CHOOZ data. We have studied the allowed parameter space resulting from these analyses as a function of the mass splitting hierarchy parameter  $\alpha = \Delta m^2 / \Delta M^2$  which parametrizes the departure from the one-dominant mass scale approximation. Finally we have studied the effect of keeping the two mass scales on the combined analysis.

Our results can be summarized as follows:

- The dominant effect of a non-vanishing value of  $\alpha$  in the atmospheric neutrino events

is an increase (decrease) of the expected number of contained  $\nu_e$  for  $\theta_{23}$  in the first (second octant) as previously discussed in Ref. [22].

- In the predicted atmospheric neutrino events the effects of a non-vanishing  $\alpha$  and of the mixing angle  $\theta_{13}$  can have opposite signs and certain degree of cancellation may occur between both effects. This particularly affects the results for Inverted schemes.
- The survival probability of  $\bar{\nu}_e$  at CHOOZ decreases for increasing values of  $\theta_{13}$  and  $\alpha$ , so that the effect of both parameters is additive in the CHOOZ reactor data. For  $\theta_{12} \leq \frac{\pi}{4}$  the effect of  $\Delta m^2$  is slightly stronger for the Normal mass ordering.
- Allowing for a non-zero value of  $\alpha$  moderately improves the quality of the atmospheric neutrino fit as a consequence of the better description of the sub-GeV electron data. This effect drives the best fit point to the first octant of the mixing angle  $\theta_{23}$ .
- Still the fit to atmospheric neutrinos is very insensitive to large values of  $\alpha$  as long as all other parameters are allowed to vary accordingly.
- As a consequence the allowed range of  $\sin^2 \theta_{13}$  and  $\sin^2 \theta_{23}$  from the atmospheric neutrino data analysis becomes, in general, broader than the one for the  $\alpha = 0$  case. This effect is more important for Inverted schemes.
- On the other hand the allowed range of  $\Delta M^2$  obtained from the atmospheric neutrino data fit is stable under departures from the one mass scale dominance approximation.
- The inclusion of the CHOOZ reactor data in the analysis leads to a stronger dependence of the results on the value of  $\alpha$ , with smaller values of  $\alpha$  and  $\theta_{13}$  favoured.
- As a consequence the final determination of the allowed ranges for both  $\Delta M^2$  and the mixing angles  $\theta_{23}$  and  $\theta_{13}$  is very robust and the ranges are only slightly different from those obtained in the one mass scale dominance approximation.

### Acknowledgments

We thank C. Peña-Garay and T. Schwetz for discussions. The work of M.M. is supported by the EU contract HPMF-CT-2000-01008. MCG-G is supported by the EU contract HPMF-CT-2000-00516. This work was also supported by the Spanish DGICYT under

grants PB98-0693 and FPA2001-3031, by the European Commission RTN network HPRN-CT-2000-00148 and by the European Science Foundation network grant N. 86.

---

- [1] Y. Fukuda *et al.*, Phys. Lett. **B433**, 9 (1998); Phys. Lett. **B436**, 33 (1998); Phys. Lett. **B467**, 185 (1999); Phys. Rev. Lett. **82**, 2644 (1999).
- [2] T. Toshito in *Moriond 2001*, XXXVI Rencontres de Moriond on Electroweak Interactions and Unified Theories (Les Arcs, France, March 2001), to appear.
- [3] S. Fukuda *et al.* [Super-Kamiokande Collaboration], hep-ex/0103032.
- [4] SNO Collaboration, Q. R. Ahmad *et al.* Phys. Rev. Lett. **87**, 071301 (2001)..
- [5] B. T. Cleveland *et al.*, Astrophys. J. **496**, 505 (1998);
- [6] SAGE Collaboration, J. N. Abdurashitov *et al.*, Phys. Rev. **C60**, 055801 (1999).
- [7] GALLEX Collaboration, W. Hampel *et al.*, Phys. Lett. **B447**, 127 (1999).
- [8] E. Bellotti, talk at XIX International Conference on Neutrino Physics and Astrophysics, Sudbury, Canada, June 2000 (<http://nu2000.sno.laurentian.ca>).
- [9] J. N. Bahcall, N. A. Bahcall and G. Shaviv, Phys. Rev. Lett. **20**, 1209 (1968); J. N. Bahcall and R. Davis, Science **191**, 264 (1976).
- [10] Z. Maki, M. Nakagawa and S. Sakata, Prog. Theo. Phys. **28**, 870 (1962); M. Kobayashi and T. Maskawa, Prog. Theor. Phys. **49**, 652 (1973).
- [11] Particle Data Group, D. E. Groom *et al.*, Eur. Phys. J. **C15**, 1 (2000).
- [12] J. N. Bahcall, M. C. Gonzalez-Garcia and C. Pena-Garay, JHEP **0108**, 014 (2001); hep-ph/0111150.
- [13] G. L. Fogli, E. Lisi, D. Montanino and A. Palazzo, Phys. Rev. D **64**, 093007 (2001); A. Bandyopadhyay, S. Choubey, S. Goswami and K. Kar, Phys. Lett. B **519**, 83 (2001); P. Krastev and A. Y. Smirnov, hep-ph/0108177; M. V. Garzelli, and C. Giunti; hep-ph/0108191. Creminelli, P., G. Signorelli, and A. Strumia, 2001, JHEP **0105**, 052.
- [14] N. Fornengo, M. C. Gonzalez-Garcia and J. W. F. Valle, Nucl. Phys. **B580** (2000) 58; R. Foot, R.R. Volkas and O. Yasuda, Phys. Rev. **D58**, 013006 (1998); O. Yasuda, Phys. Rev. **D58**, 091301 (1998); E.Kh. Akhmedov, A. Dighe, P. Lipari and A.Yu. Smirnov, Nucl. Phys. **B542**, 3 (1999).
- [15] G.L. Fogli, E. Lisi and A. Marrone, Phys. Rev. D **64**, 093005 (2001).
- [16] M. C. Gonzalez-Garcia, M. Maltoni, C. Pena-Garay and J. W. Valle, Phys. Rev. D **63**, 033005 (2001).

- [17] G. L. Fogli, E. Lisi, A. Maronne and G. Scioscia, Phys. Rev. **D59**, 033001 (1999); G.L. Fogli, E. Lisi, D. Montanino and G. Scioscia Phys. Rev. **D55**, 4385 (1997); A. De Rujula, M.B. Gavela, P. Hernandez, Phys. Rev. **D63**, 033001 (2001); T. Teshima, T. Sakai, Phys. Rev. D **62**, 113010 (2000).
- [18] G.L. Fogli, E. Lisi, D. Montanino, Phys. Rev. **D54**, 2048 (1996); G. L. Fogli, E. Lisi, D. Montanino and A. Palazzo, Phys. Rev. **D62**, 113004 (2000) ; A.M. Gago, H. Nunokawa, R. Zukanovich Funchal; Phys. Rev. D **63**, 013005 (2001).
- [19] M. Apollonio, *et al.*, CHOOZ Coll., Phys. Lett. **B 466**, 415 (1999).
- [20] S. M. Bilenky, D. Nicolo and S. T. Petcov, hep-ph/0112216; S. T. Petcov and M. Piai, hep-ph/0112074.
- [21] I. Mocioiu and R. Shrock, JHEP 0111, 050 (2001)
- [22] O. L. Peres and A. Y. Smirnov, Phys. Lett. B **456**, 204 (1999); hep-ph/0201069.
- [23] A. Strumia, JHEP **04**, 26 (1999).
- [24] M. Narayan and S. Uma Sankar, hep-ph/0111108. T. Sakai and T. Teshima, Prog. Theor. Phys. **102**, 629 (1999).
- [25] A. Marrone, talk at the NOON 2001 workshop, (<http://www-sk.icrr.u-tokyo.ac.jp/noon2001>).
- [26] M. Ambrosio *et al.*, MACRO Coll., Phys. Lett. B **517**, 59 (2001).
- [27] J. Gluza and M. Zralek, Phys. Lett. B **517**, 158 (2001).
- [28] J. Schechter and J. W. F. Valle, Phys. Rev. **D24**, 1883 (1981) and Phys. Rev. **D25**, 283 (1982); L. Wolfenstein, Phys. Lett. **B107**, 77 (1981).
- [29] E. Lisi and D. Montanino, Phys. Rev. **D56**, 1792 (1997).
- [30] A.M. Dziewonski and D.L. Anderson, Phys. Earth Planet. Inter. **25**, 297 (1981).
- [31] C. Peña-Garay, private communication.

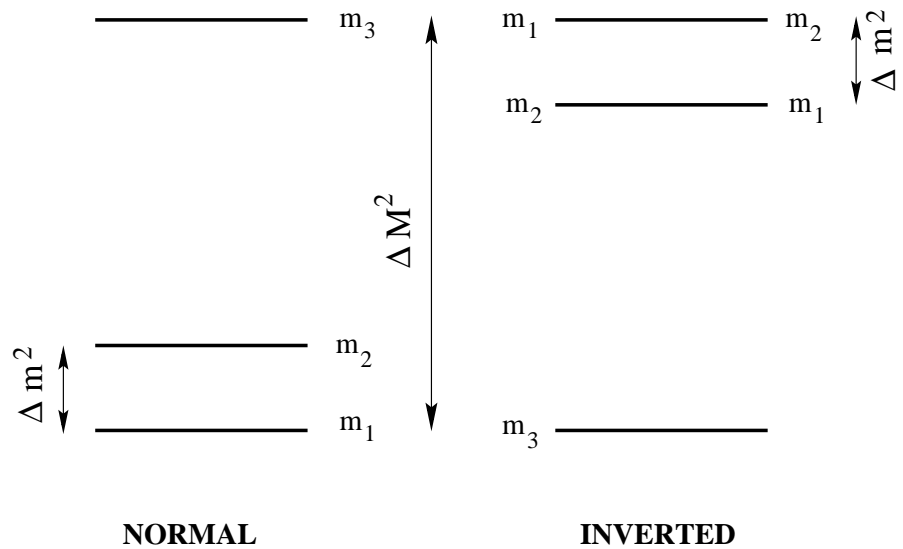


Figure 1: Our convention for the mass splitting and ordering.

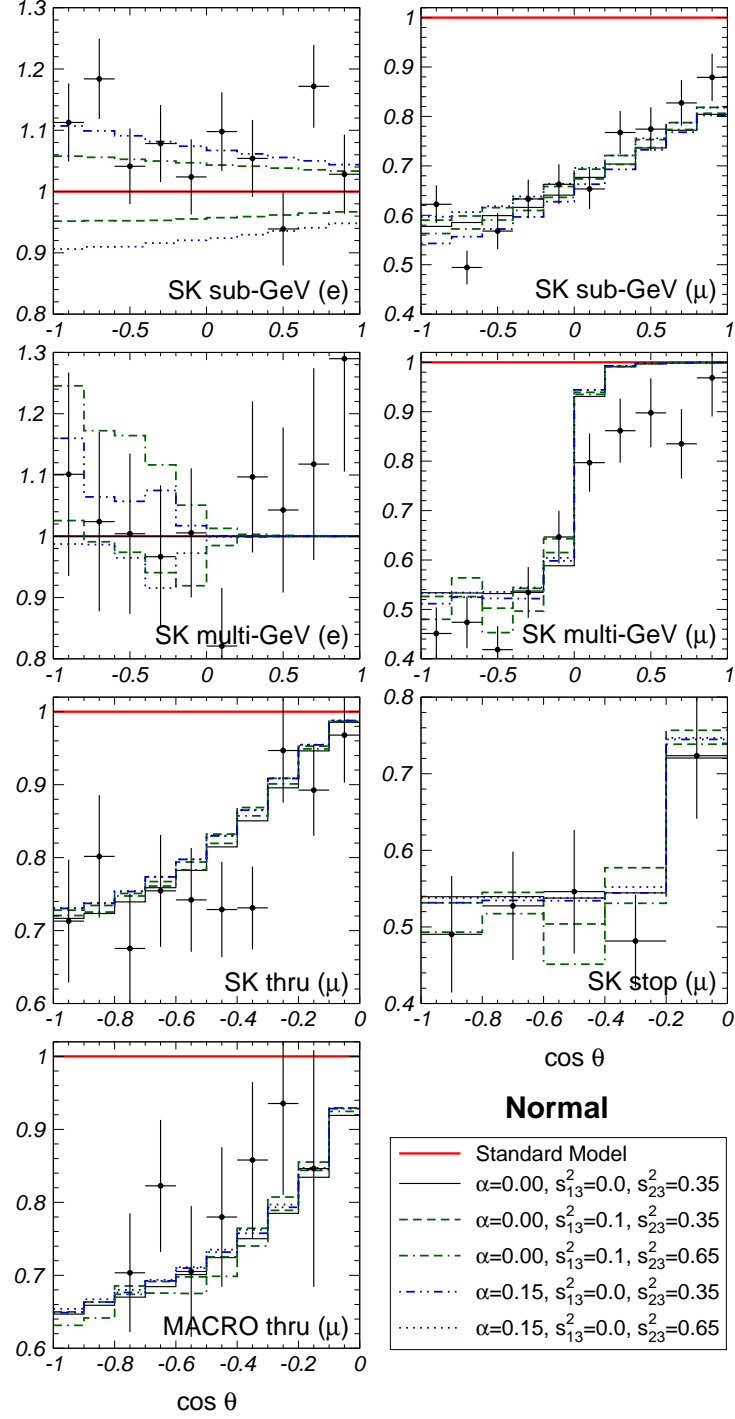


Figure 2: Zenith-angle distributions (normalized to the no-oscillation prediction) for the Super-Kamiokande  $e$ -like and  $\mu$ -like contained events, for the Super-Kamiokande stopping and through-going muon events and for Macro upgoing muons. The various dashed lines are the expected distributions for the Normal mass ordering with  $\Delta M^2 = 3 \times 10^{-3} \text{ eV}^2$ ,  $\tan^2 \theta_{12} = 1/3$  and several values of  $\sin^2 \theta_{13}$  and  $\sin^2 \theta_{23}$  as given in the figure.

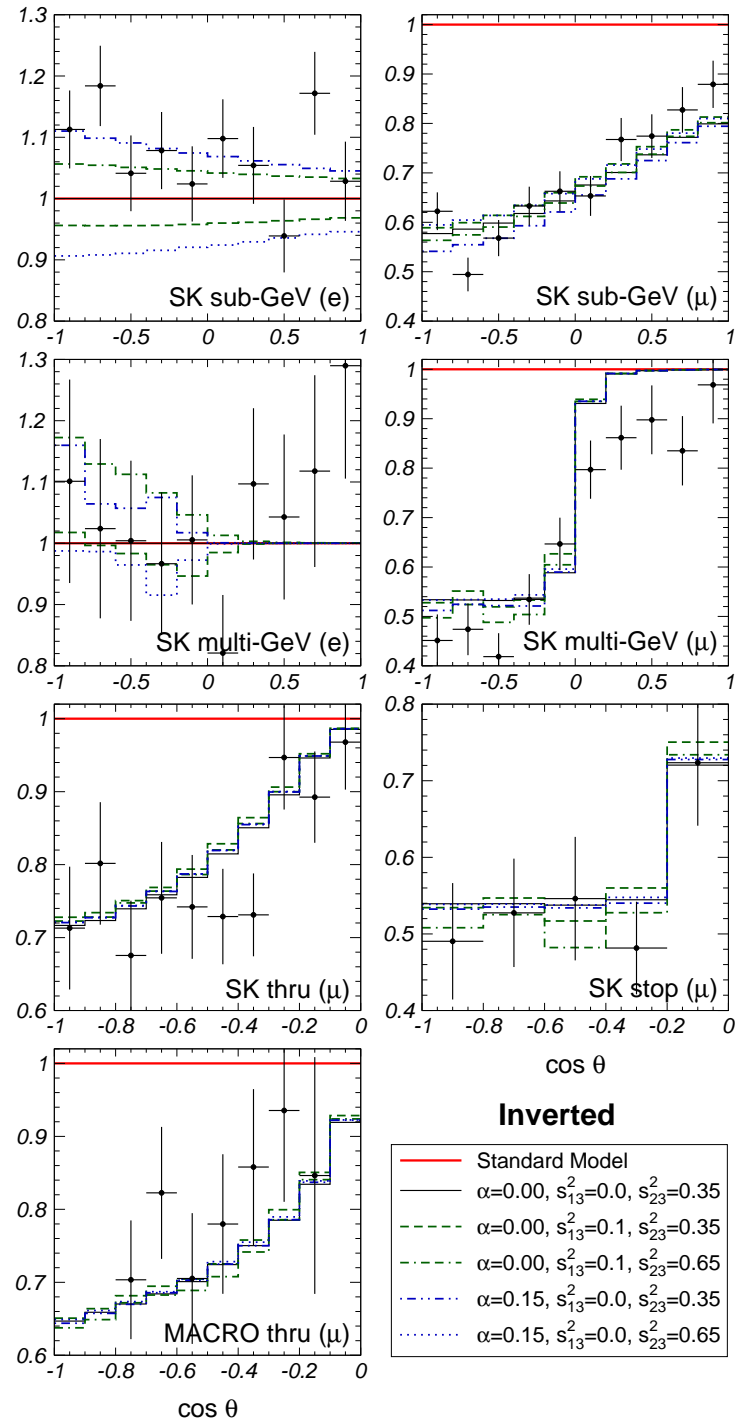


Figure 3: Same as Fig. 2 but for Inverted mass ordering.

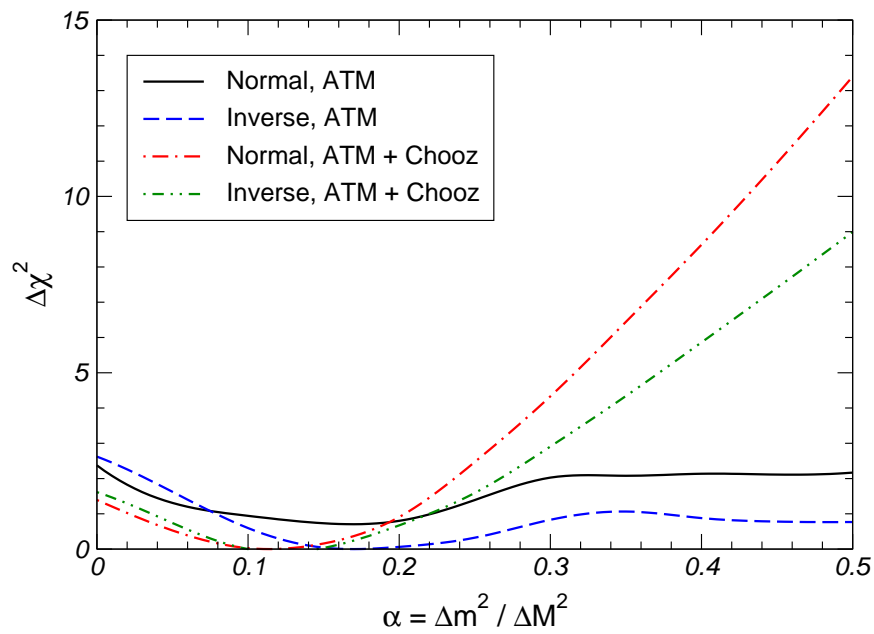


Figure 4: Dependence of  $\Delta\chi^2$  on the mass splitting parameter  $\alpha$  for  $\tan^2 \theta_{12} = 1/3$ , for the analysis of atmospheric neutrinos alone and also in combination with the CHOOZ reactor data.

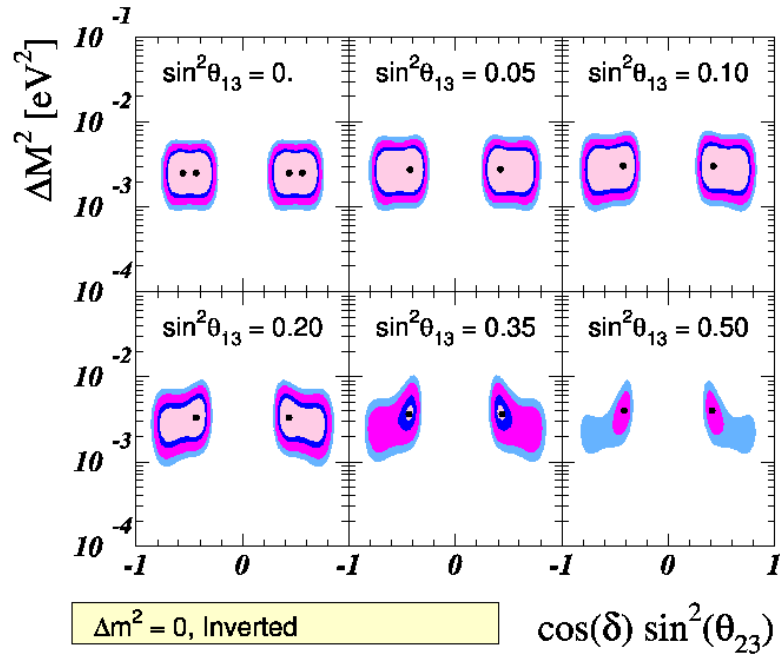
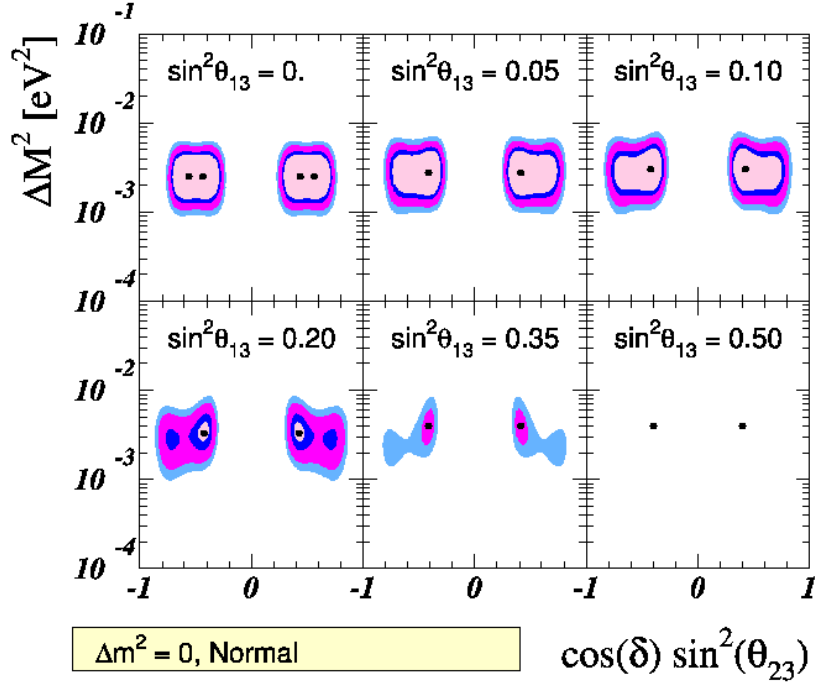


Figure 5: 90%, 95%, 99% and  $3\sigma$  allowed regions in the  $(\sin^2 \theta_{23}, \Delta M^2)$  plane for different  $\sin^2 \theta_{13}$  from the analysis of the atmospheric neutrino data, in the one mass scale dominance approximation  $\alpha = 0$ . The local minima are marked with a dot.

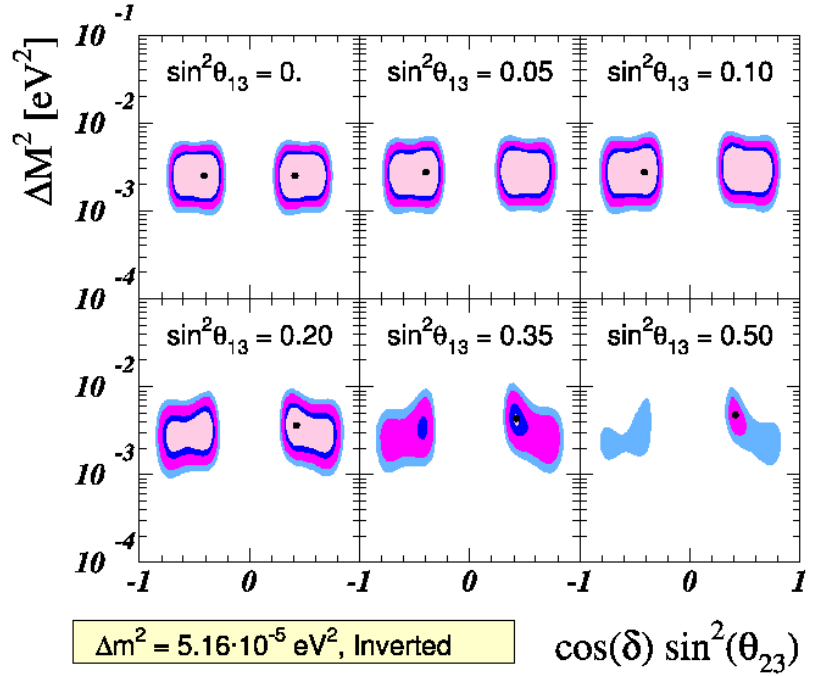
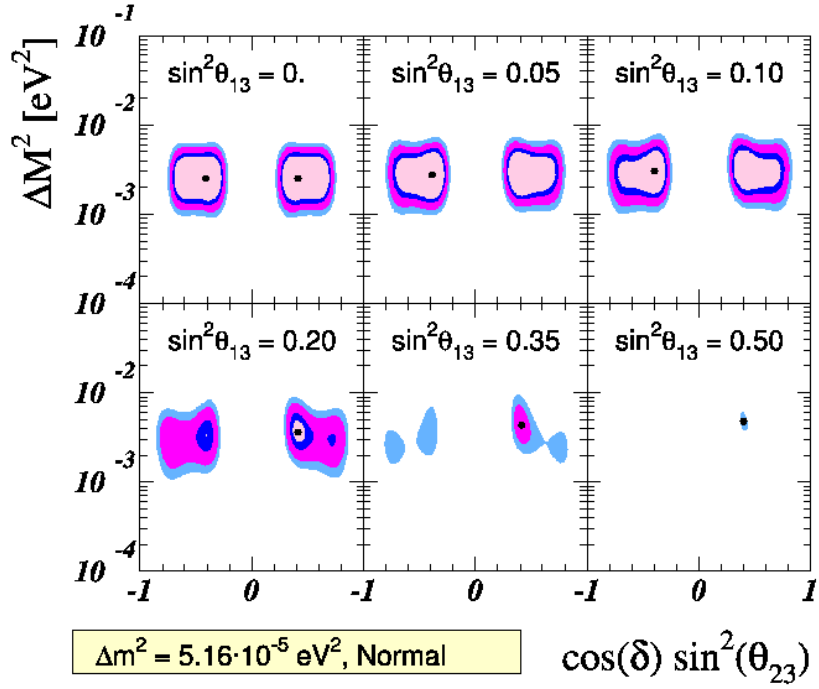


Figure 6: 90%, 95%, 99% and  $3\sigma$  allowed regions in the  $(\cos \delta \sin^2 \theta_{23}, \Delta M^2)$  plane for different  $\sin^2 \theta_{13}$  from the analysis of the atmospheric neutrino data with two mass scales. We fix  $\tan^2 \theta_{12} = 1/3$  and  $\Delta m^2 = 5.2 \times 10^{-5}$  eV $^2$ , corresponding to the best fit point of the solar neutrino analysis. The local minima are marked with a dot.

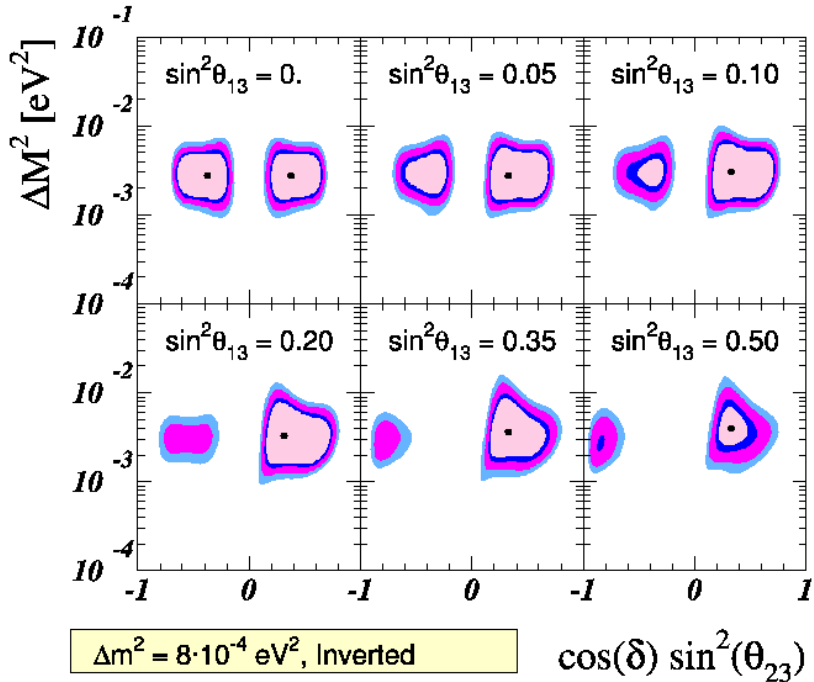
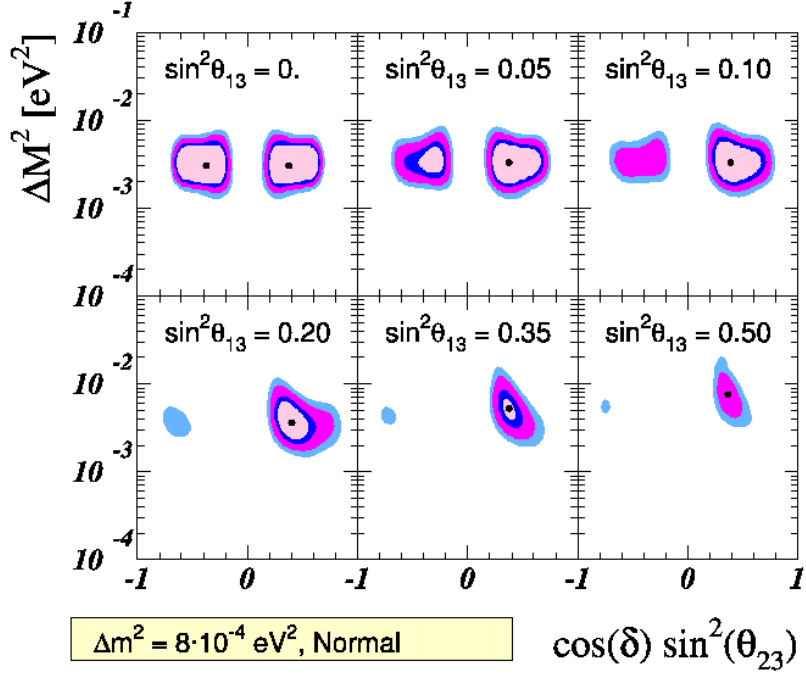


Figure 7: 90%, 95%, 99% and  $3\sigma$  allowed regions in the  $(\cos \delta \sin^2 \theta_{23}, \Delta M^2)$  plane for different  $\sin^2 \theta_{13}$  from the analysis of the atmospheric neutrino data with two mass scales. We fix  $\tan^2 \theta_{12} = 1/3$  and  $\Delta m^2 = 8 \times 10^{-4} \text{ eV}^2$ , corresponding to the maximum scale allowed by the solar+CHOOZ neutrino analysis. The local minima are marked with a dot.

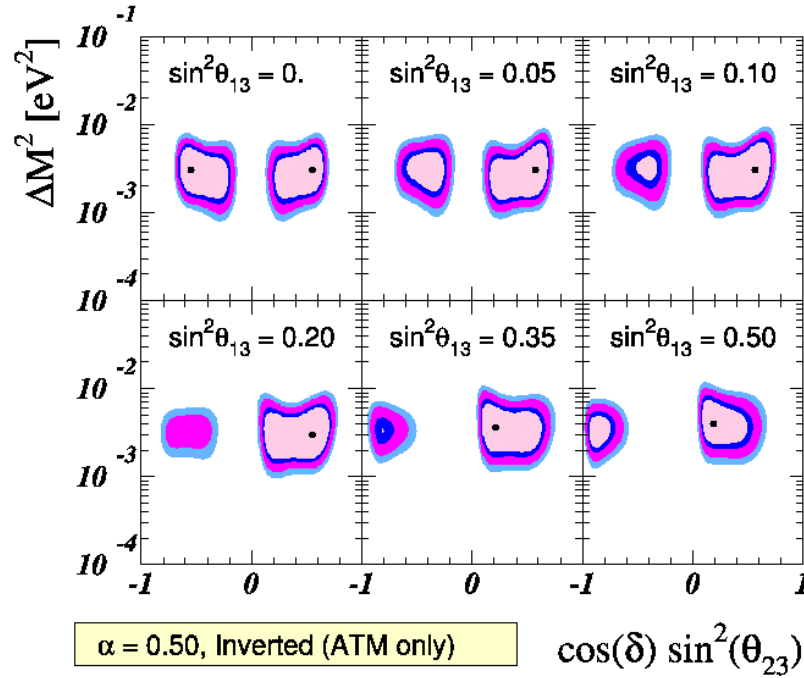
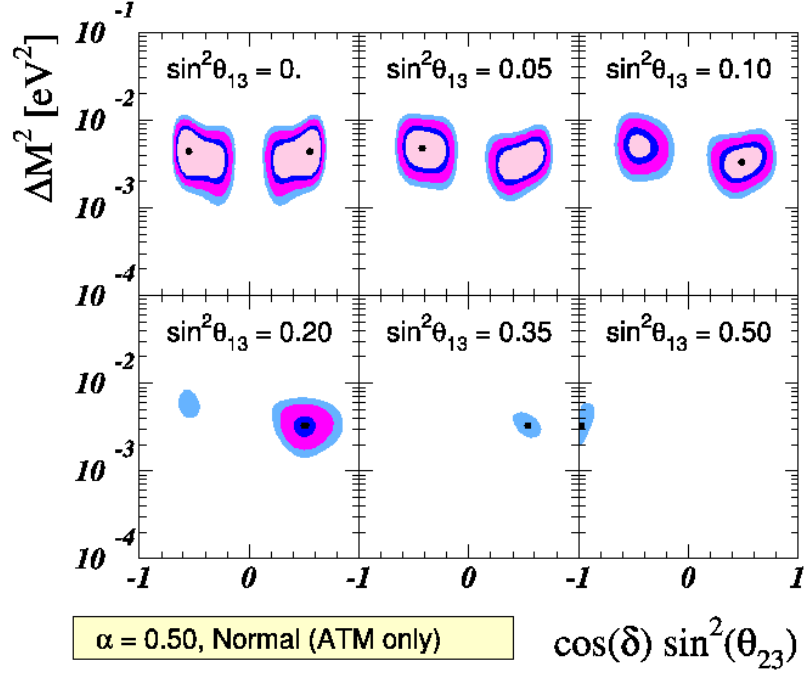


Figure 8: 90%, 95%, 99% and  $3\sigma$  allowed regions in the  $(\cos \delta \sin^2 \theta_{23}, \Delta M^2)$  plane for different  $\sin^2 \theta_{13}$  from the analysis of the atmospheric neutrino data, in the “democratic” scenario  $\alpha = 0.5$  and with  $\tan^2 \theta_{12} = 1/3$ . The local minima are marked with a dot.

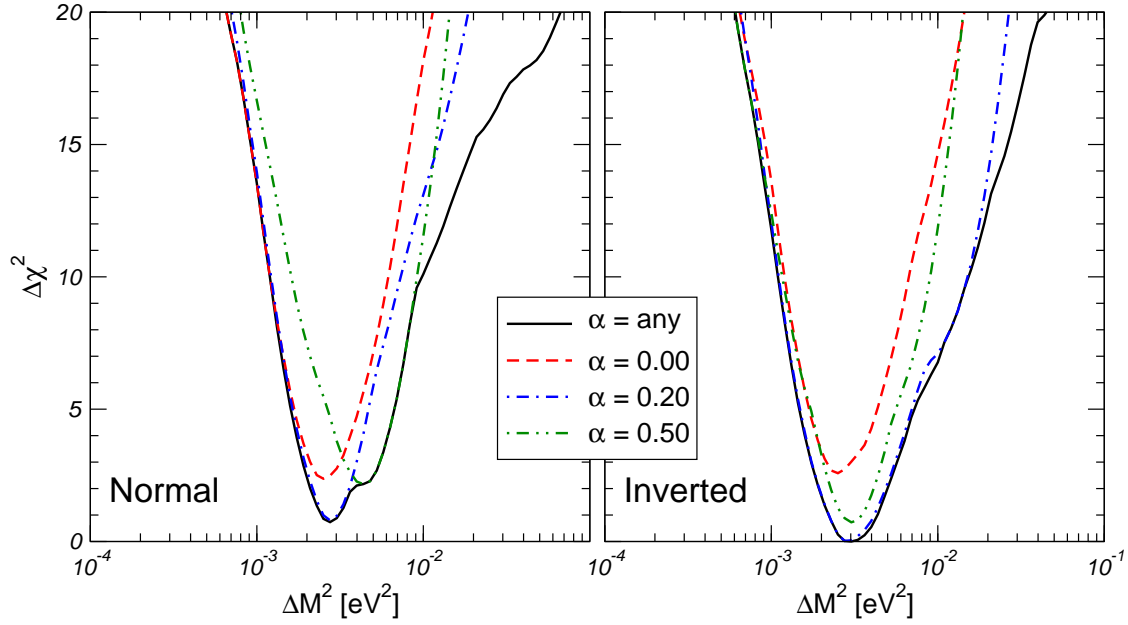


Figure 9: Dependence of the  $\Delta\chi^2$  on the large mass scale  $\Delta M^2$  for different values of  $\alpha$  and for the Normal (left panel) and Inverted (right panel) cases. See text for details.

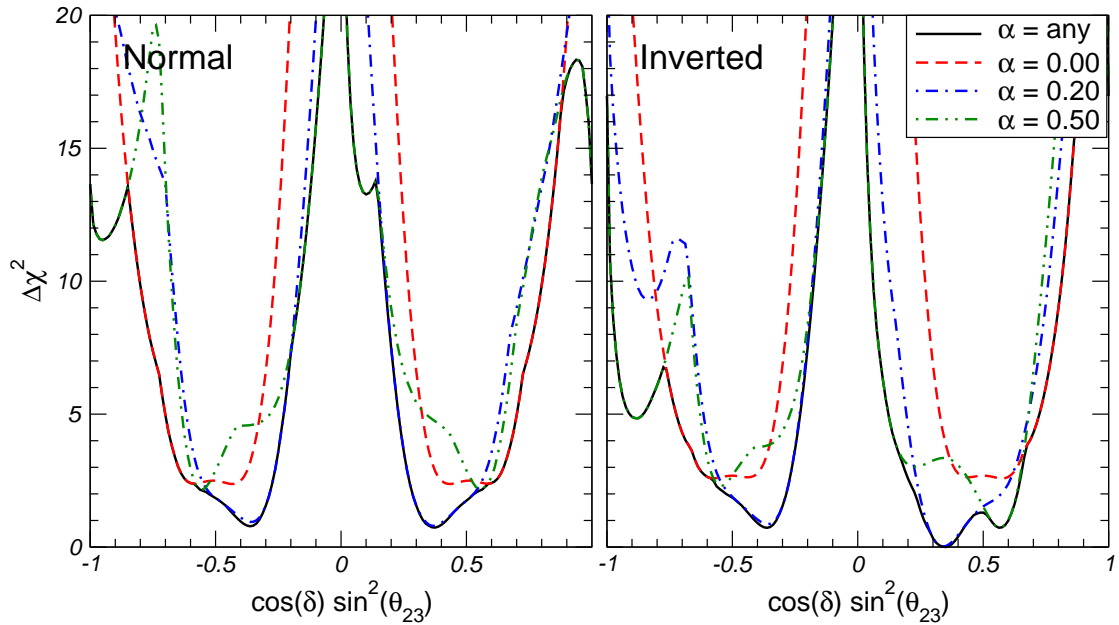


Figure 10: Dependence of the  $\Delta\chi^2$  on the large mass scale  $\cos\delta \sin^2\theta_{23}$  for different values of  $\alpha$  and for the Normal (left panel) and Inverted (right panel) cases. See text for details.

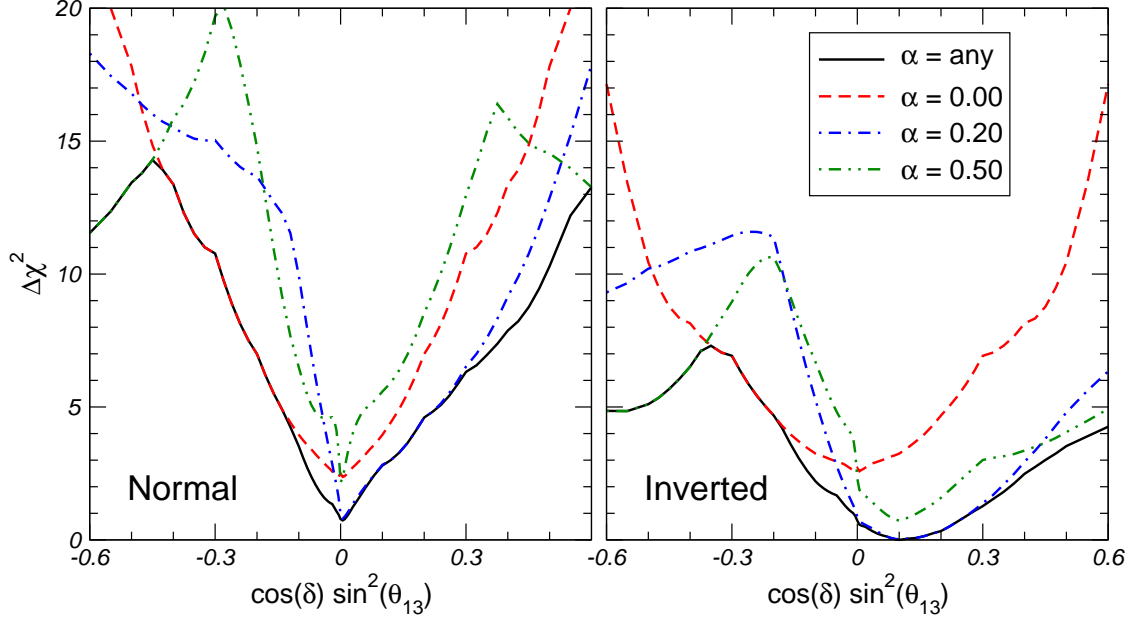


Figure 11: Dependence of the  $\Delta\chi^2$  on the large mass scale  $\cos\delta\sin^2\theta_{13}$  for different values of  $\alpha$  and for the Normal (left panel) and Inverted (right panel) cases. See text for details.

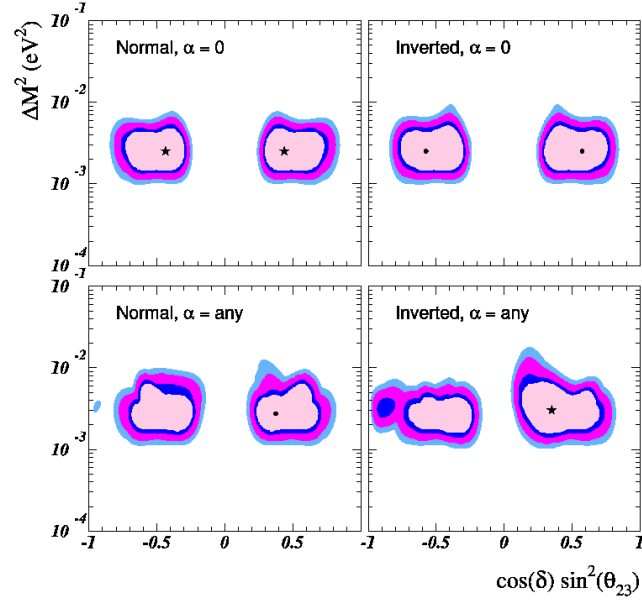


Figure 12: 90%, 95%, 99% and  $3\sigma$  allowed regions in the  $(\cos\delta\sin^2\theta_{23}, \Delta M^2)$  from the analysis of the atmospheric neutrino data for the Normal (left panels) and Inverted (right panels) cases, for  $\tan^2\theta_{12} = 1/3$  and for arbitrary values of  $\theta_{13}$  and  $\alpha$  (lower panels). See text for details. The upper panels correspond to the case  $\alpha = 0$ . The best fit point in each case is marked with a star. The local minima are marked with a dot.

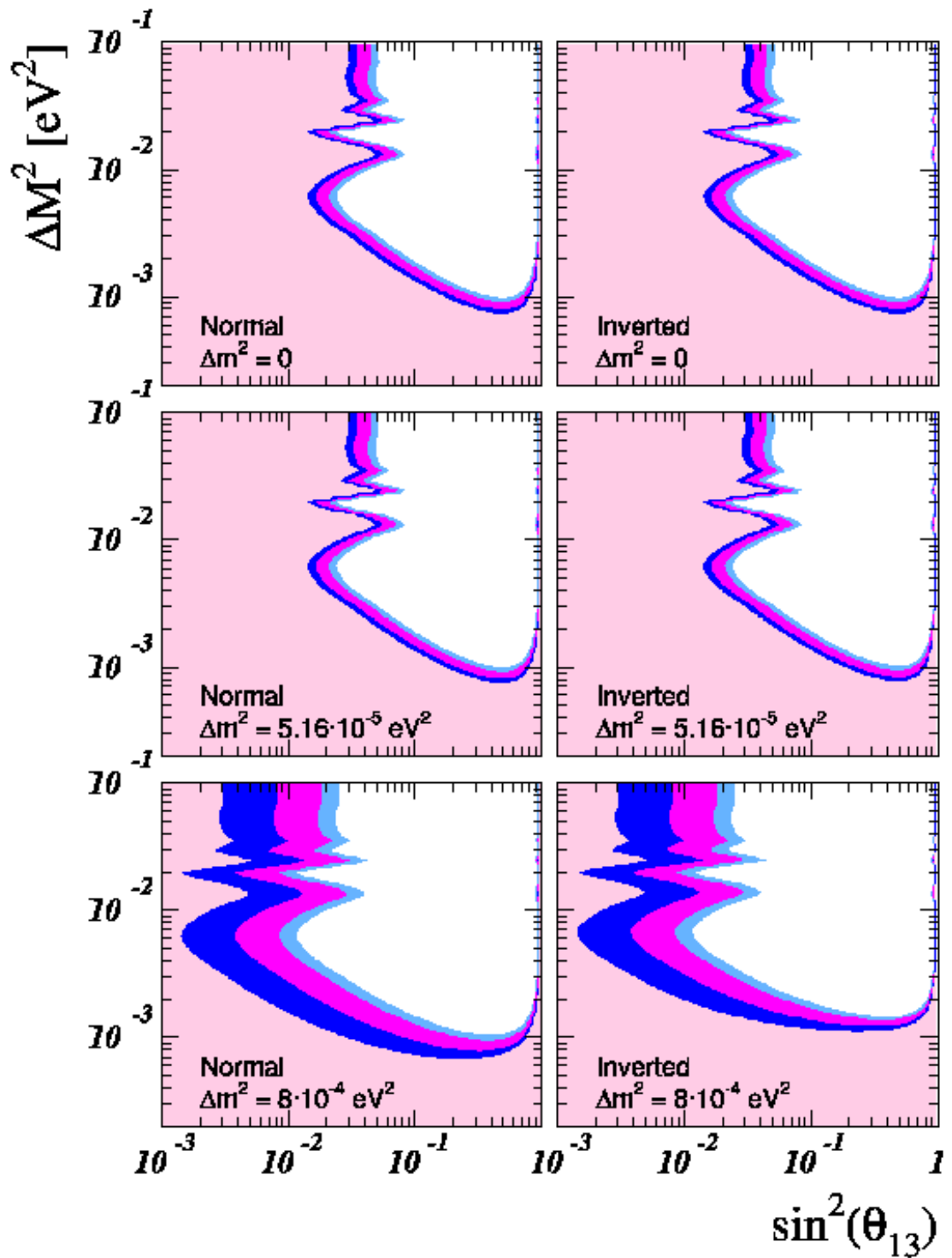


Figure 13: 90%, 95%, 99% and  $3\sigma$  (2 d.o.f.) allowed regions from the analysis of the CHOOZ reactor data in the  $(\sin^2 \theta_{13}, \Delta M^2)$  plane for different values of  $\Delta m^2$  ( $\tan^2 \theta_{12} = 1/3$ ), for the Normal (left panels) and Inverted (right panels) cases.

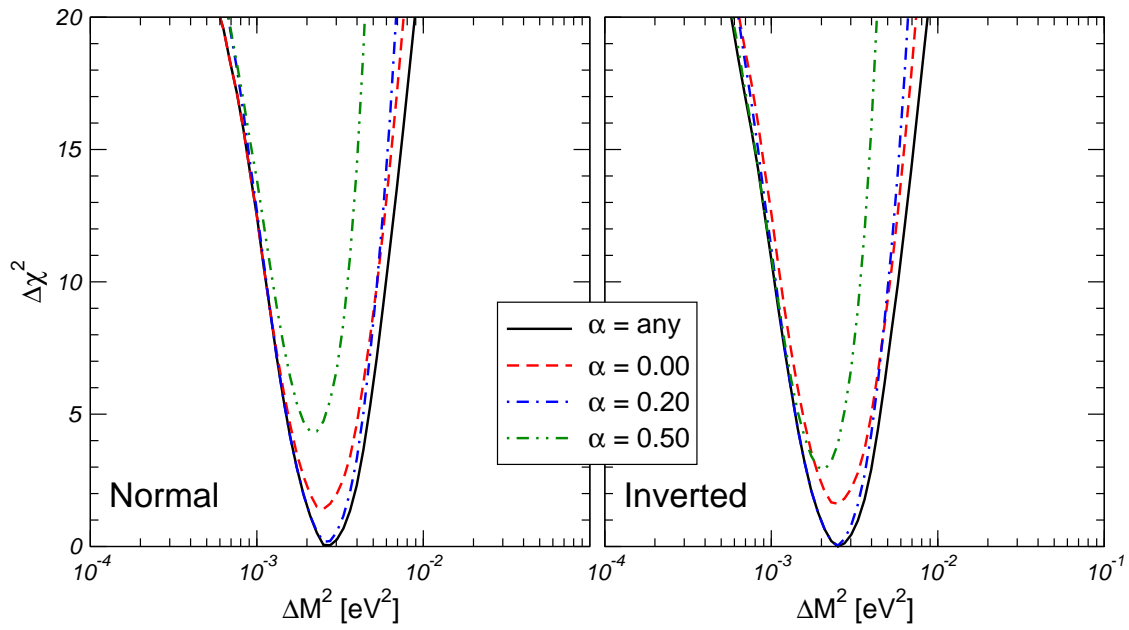


Figure 14: Same as Fig. 9 but including also the CHOOZ result.

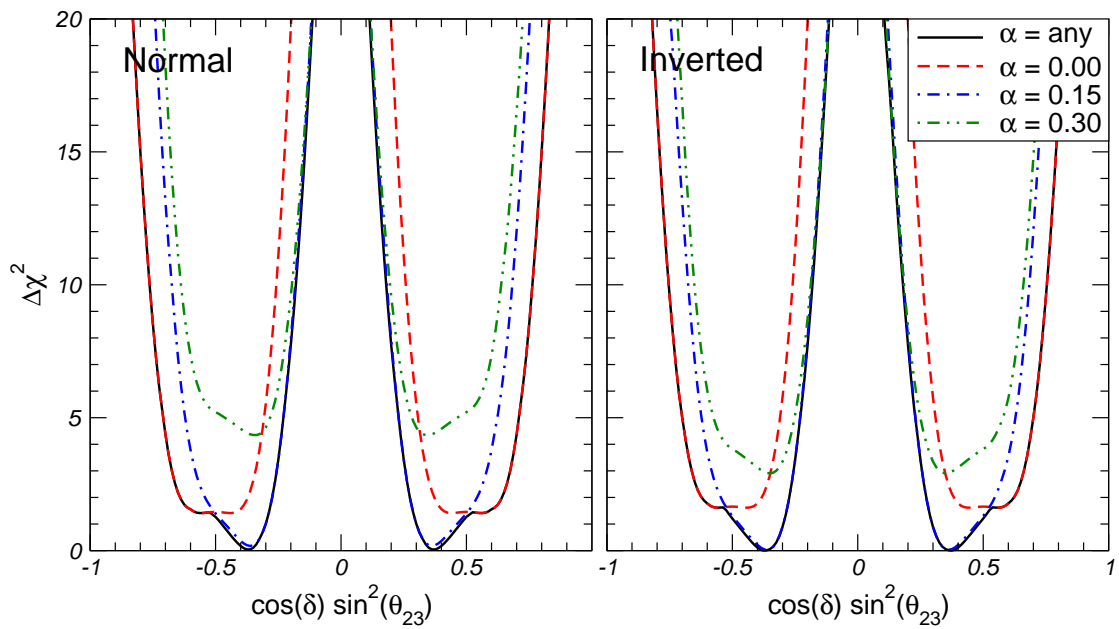


Figure 15: Same as Fig. 10 but including also the CHOOZ result.

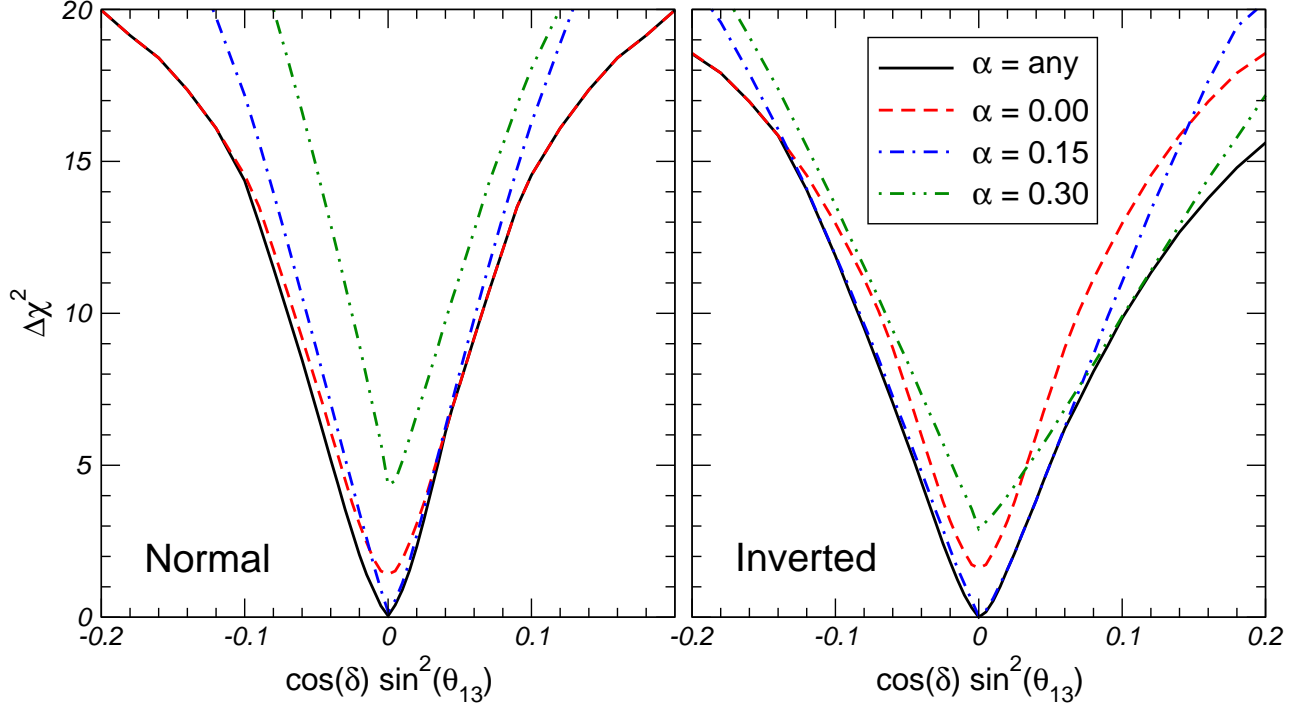


Figure 16: Same as Fig. 11 but including also the CHOOZ result.

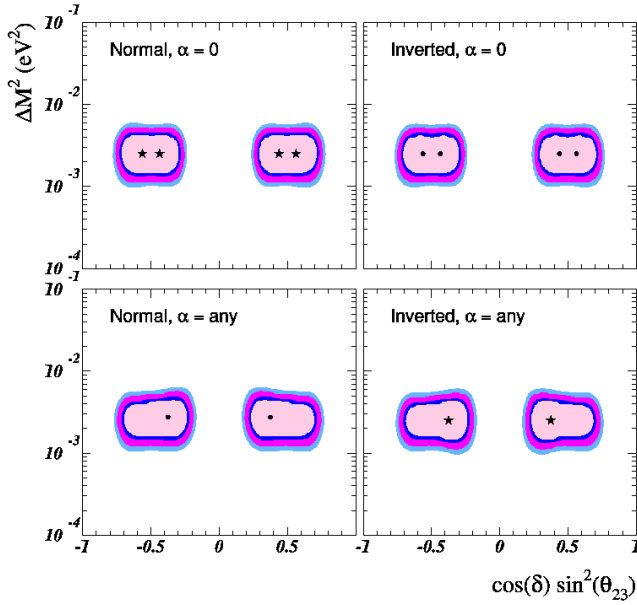


Figure 17: 90%, 95%, 99% and  $3\sigma$  allowed regions in the  $(\cos \delta \sin^2 \theta_{23}, \Delta M^2)$  from the analysis of the atmospheric and CHOOZ neutrino data with  $\tan^2 \theta_{12} = 1/3$ , for the Normal (left panels) and Inverted (right panels) cases and for arbitrary values of  $\theta_{13}$  and  $\alpha$  (lower panels). See text for details. The upper panels correspond to the case  $\alpha = 0$ . The best fit point in each case is marked with a star. The local minima are marked with a dot.